Malaysian Journal of Catalysis 3 (2018) 48-53

Malaysian Journal of Catalysis
http://mjcat.utm.my/
MJCat
Research Article

Characterization of Ni catalyst supported on α-Al_2O_3 and SiO_2 for syngas production via dry reforming of glycerol

Norazimah Harun[a], Sumaiya Zainal Abidin[a,b]*, Nur Nabillah Mohd Arif[a], Nurul Aini Mohamed Razali[a], Mohammad Tazli Azizan[c]
[a]*Faculty of Chemical & Natural Resources Engineering, Universiti Malaysia Pahang, 26300 Gambang, Pahang, Malaysia.*
[b]*Centre of Excellence for Advanced Research in Fluid Flow (CARIFF),Universiti Malaysia Pahang, 26300 Gambang, Pahang, Malaysia.*
[c]*Department of Chemical Engineering, Faculty of Engineering, Universiti Teknologi PETRONAS, 32610 Bandar Seri Iskandar, Perak Darul Ridzuan, Malaysia*
** Corresponding author e-mail: sumaiya@ump.edu.my*

Article history :
Received 9 August 2017
Accepted 30 November 2017

GRAPICAL ABSTRACT

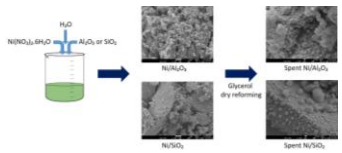

ABSTRACT

Ni-based catalysts supported on α-Al_2O_3 and SiO_2 were synthesized using the wet impregnation method. Glycerol dry reforming to produce hydrogen (H_2), carbon monoxide (CO) and methane (CH_4) was carried out in a tubular reactor at 973 K under atmospheric pressure. The catalysts were characterized using X-Ray Diffraction, Bruneuer-Emmet Teller surface area, Thermogravimetric Analysis, temperature-programmed reduction and Scanning Electron Microscopy. Ni/Al_2O_3 gave higher glycerol conversion and H_2 yield (14.46% and 9.82% respectively) compared to Ni/SiO_2. The better performance was due to the smaller crystallite size and higher specific surface area of Ni/Al_2O_3 compared to Ni/SiO_2. In addition, the structure of Al_2O_3 also improved the activity and the stability of this catalyst, by creating a platform for uniform metal dispersion as well as inhibition of carbon deposits. The encapsulating carbon and filamentous carbon deposits could be observed on Ni/Al_2O_3 and Ni/SiO_2, respectively, which can be easily removed through oxidation.

Keywords: Glycerol; Dry reforming; Syngas; Nickel-based catalysts; Silicon Oxide; Aluminium Oxide

| eISSN 0128-2581 |

1. INTRODUCTION

Renewable energy such as biodiesel in particular have been gaining attention as alternative energy sources due to the depletion of fossil-based resources, rapid increase of oil demand and significant contribution of conventional fuel to the greenhouse effect. Biodiesel possess several advantages compared to conventional diesel i.e. apart from biodiesel being a renewable energy source with lower carbon emissions, biodiesel contains no sulphur and aromatic substances [1].

Biodiesel is produced through the transesterification of triglyceride and approximately 10 wt% of crude glycerol constitutes the total product [2]. The abundance of glycerol worldwide resulting from the high demand in biodiesel production has led to the discovery of viable alternatives to utilize glycerol as a feedstock. One of the ways is the production of hydrogen (H_2) and syngas (H_2: CO) through gasification and catalytic reforming of glycerol. Syngas is widely used as an intermediate in producing synthetic natural gas, petroleum, ammonia and methanol [3, 4]. The most common method to produce H_2 and H_2: CO is steam reforming. However, compared to dry reforming of methane, this method requires high-energy consumption in order to obtain optimum reaction conditions and products yield [3]. The glycerol dry reforming process is considered as an attractive process because it converts CO_2, which is a greenhouse gas into a synthesis gas and simultaneously removes it from the carbon biosphere cycle [5].

Wang et al. (2009) pioneered the glycerol dry reforming study by conducting a thermodynamic analysis using the Gibbs energy minimization method. From their study, it was found that H_2, CO, CO_2, CH_4, H_2O and carbon (solid deposition) are the likely products of the process [5]. In addition, atmospheric pressure is preferable for the system due to the high H_2 concentration produced at lower pressure and also, higher pressure promotes the formation of side reactions [6]. Moreover, CO_2 conversion increases with the increase of reaction temperature. At 1000 K and CO_2: glycerol molar ratio of 1:1, 100% conversion of glycerol was achieved with maximum production of syngas, where 6.4 moles of syngas was produced per mole of glycerol [5].

Lee and co-workers focused on the synthesis and characterization of Ni-based catalyst supported on different oxides (cement clinker and alumina) for glycerol dry reforming. In their study, lanthanum was incorporated as a promoter to enhance the performance of the catalysts. The reaction successfully produced H_2, CO, CH_4 and trace of gases, with H_2: CO ratio 2.0 suitable for Fischer-Tropsch synthesis. The maximum glycerol conversion and H_2 yield were achieved at the best reaction conditions of 1:1 molar ratio of CO_2: glycerol, atmospheric pressure and reaction temperature higher than 973 K [7-11].

Undoubtedly, the selection of suitable catalyst is crucial in catalytic reforming process. Although Pt and Pd are often used in many reforming activities, Ni-based catalyst is more practical due to its abundance and low cost. However, these catalysts are also known to favor the deposition of carbon (coking), which may reduce the performance of the catalysts. The coking problem of Ni catalyst could be overcome by supporting the nickel with oxides or introducing metal promoter into the catalyst structure. This alternative could promote H_2 production and improve the durability of the catalyst. In addition, it will simultaneously reduce the carbon deposition on the active surface of the catalyst.

Alumina has been widely used in many reforming studies as catalyst support due to the nature of alumina that provides high specific surface area, mechanical strength and stability. γ-alumina is often used in many reforming studies due to these characteristics. However, α-alumina is the most stable type of alumina (α-Al_2O_3) and it is the final product of thermal or dehydroxylation treatments of hydroxides [12]. Furthermore, according to Ross et al. (1996), α-Al_2O_3 also

has high mechanical and thermal stability. Silica has the similar characteristic with alumina in term of the amphoteric behaviour. However, compared to alumina, silica is weak in acidity [13].

From previous literatures, to the best of our knowledge, both catalysts support have not been used in any dry glycerol reforming reaction. Therefore, this paper aims to study the performance of Ni catalyst impregnated on both supports. It will focuses on CO_2 dry reforming of glycerol over Ni-based catalyst supported on α-Al_2O_3 and silicon oxide (SiO_2) at 15wt% Ni-loading. The characterization and reaction studies for both catalysts were carried out to determine the best performing catalyst for the production of syngas.

2. EXPERIMENTAL

2.1 Catalyst preparation

Prior to the synthesis using the wet impregnation method, alumina (Acros Organics, 99% purity) and silica (Acros Organics, 99% purity) was ground, sieved to 250 µm particle size and calcined at 1073 K for 6 h, with ramping rate of 5 K min^{-1}. These procedures were employed to remove the impurities and avoid the phase transition associated with at high temperature during reforming process. The calcined oxide supports were then impregnated with an aqueous solution of Ni $(NO_3)_2.6H_2O$ (Acros Organics, 99% purity) of 15 wt % Ni-loading. The solutions were stirred for 3 h at ambient temperature, dried overnight in the oven at temperature of 373 K. During the drying process, the slurries were manually stirred every 1 h for the initial 6 h using a glass rod to avoid particle agglomeration. The dried compound was calcined in the furnace at 773 K for 5 h employing heating rate of 5 K min^{-1}. The catalysts were cooled down, ground and sieved using 150 µm sieve size.

2.2 Catalysts characterization

The surface structure and morphology of the catalysts were analyzed by using Scanning Electron Microscopy (SEM) JOEL.JSM- 7800F model. Brunauer-Emmet-Teller (BET) analysis was carried out using Thermo-Scientific Surfer to determine the specific surface area of the calcined catalysts. X-Ray Diffraction (XRD) analysis was conducted using Rigaku Miniflex II to obtain crystalline structure of the catalysts. The analysis was carried out using CuKα radiation (λ = 1542 Å) at 15 mA and 30 kV. The scan rate was 1° min^{-1} for 2θ range of 10° - 80°. The crystallite size was calculated using Scherrer equation represented in Equation 1 [14];

$$d = \frac{K\lambda}{\beta cos\theta} \quad (1)$$

where d is the crystallite size, λ is the X-ray radiation ($\lambda = 0.154\ nm$), β is the full-width at half maximum (FWHM) and θ is half of diffraction angle. Thermogravimetric analysis was conducted using the Q500-model thermogravimetry analyser, with ramping rate at 10 K min^{-1}. The temperature-programmed reduction (TPR) profiles of the catalysts under H_2-blanket were carried out using Thermo Finnigan TPDRO. The ramping rate was fixed at 10 K min^{-1}, increasing the temperature from room temperature to 1173 K followed by 1 h holding time. For TPD-NH_3, the sample was put in the tube and pre-treated in an oven at room temperature. Prior to analysis, the catalyst was placed in reactor tube and heated under helium gas at a flow rate of 30 ml/min flow until it reached 500 °C and immediately cooled to 100 °C. Then, the sample was flowed with 3% NH_3 for 1 h and flushed with helium again at the same condition. In this analysis, the heating rate was set at 10 K min^{-1} with 1 h holding period. The tube was subjected for the second pre-treatment and further subjected to temperature raise up to 1173 K.

2.3 Dry reforming experimental work

Glycerol dry reforming was carried out in a stainless-steel fixed bed reactor (ID = 0.95 cm; length 40 cm). The reaction was conducted at 973 K and atmospheric pressure with CO_2 to glycerol molar ratio of 1:1. The volumetric flow rate of glycerol and CO_2 were fixed at 0.03 ml min^{-1} and 100 ml min^{-1}, respectively. Prior to reforming reaction, 0.2 g of the catalyst was reduced at 973 K under 50 ml min^{-1} of H_2 for 1 h. Glycerol (Fisher Scientific, 99.95% purity) was introduced to the reactor using the HPLC pump. The outlet gases were passed through a silica gel flask to absorb moisture content. The effluent gas was collected using gas sampling bag. The composition of syngas produced was analyzed using Agilent 6890 Series gas chromatograph equipped with thermal conductivity detector and capillary column, HP-MOLSIV (30.0 m × 530 µm × 40.0 µm). The column was operated at 353 K with Helium as a carrier gas, while oven temperature was maintained at 393 K.

2.4 Reaction metrics

The catalyst performance was evaluated based on the glycerol conversion and H_2 yield. The glycerol conversion to gaseous products was determined based on the atomic H-balance and defined as shown in Equation 2:

$$X_G(\%) = \frac{2F_{H_2} \times 4F_{CH_4}}{8F_{C_3H_8O_3}} x100 \quad (2)$$

The yield of hydrogen is expressed as in Equation 3:

$$Y_{H_2}(\%) = \frac{2F_{H_2}}{8F_{C_3H_8O_3}} \times 100 \quad (3)$$

The yield of C-containing yield is expressed as in Equation 4 (i = CO, CH_4):

$$Y_i(\%) = \frac{F_i}{3F_{C_3H_8O_3}} \times 100 \quad (4)$$

where F_{H_2} and F_{CH_4} represents the molar flow rate of hydrogen and methane product respectively while $F_{C_3H_8O_3}$ refers to the molar flow rate of the inlet glycerol.

3. RESULTS AND DISCUSSION

3.1 Characterization Study

Figure 1 shows the crystalline structures of the Ni/Al_2O_3 and Ni/SiO_2 catalysts. The diffractogram peaks reveals that the crystalline phase associated with NiO at 2θ of 37.2°, 43.3° and 62.8° were observed for both catalysts [7, 15]. The XRD patterns for Ni/Al_2O_3 shows the thin and high peaks representing NiO and Al_2O_3. The peaks observed at 2θ of 37.2°, 43.3° and 62.8° for Ni/Al_2O_3 catalyst was due to the formation of $NiAl_2O_4$ species in the catalyst system. The characteristic peaks of Al_2O_3 crystallites were observed at 25.6°, 35.1°, 37.7°, 52.6°, 57.5°, 61.1°, 66.5° and 68.2°. The low intensity peak of NiO crystallites at 37.2°, 43.3°, 62.8°, 75.4° and 79.4° for Ni/SiO_2 catalyst was indicative of low interaction between Ni and silica support. SiO_2 peak appeared at 2θ value of 21.5° and co-exist with NiO peaks at 37.2° and 62.8°. The metal particles size of Ni/Al_2O_3 and Ni/SiO_2 calculated using the Scherrer equation were between 6.1 – 24.5 nm and 7.1 – 33.0 nm, respectively. The weak peaks indicate the formation of small crystalline particles, which might cover the active sites of the catalyst [7].

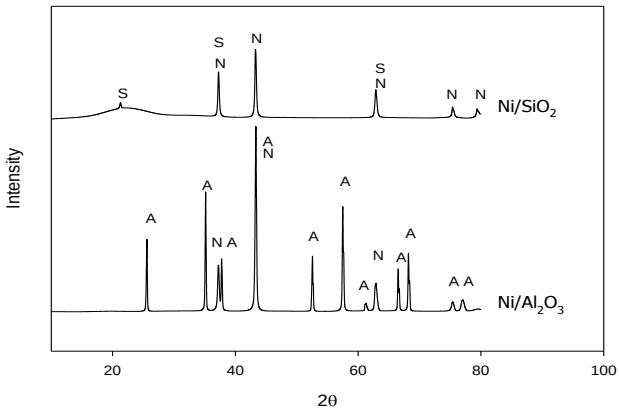

Figure 1 XRD pattern for Ni/Al_2O_3 and Ni/SiO_2 (A-Al_2O_3, S-SiO_2 and N-NiO)

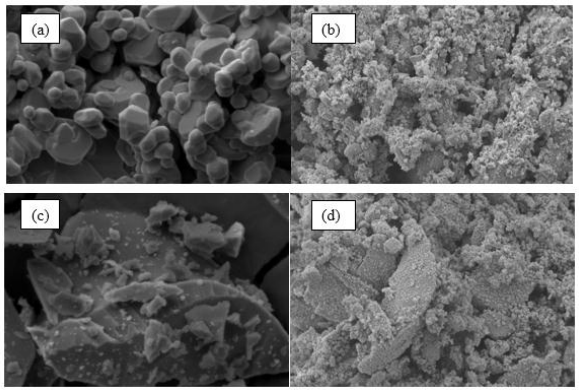

Figure 2 Morphology structure of (a) Al_2O_3, (b) Ni/Al_2O_3, (c) SiO_2, and (d) Ni/SiO_2 at 5000x magnification.

The morphology structures of the catalysts at 5000 × magnifications are shown in Figure 2. The calcined Al_2O_3 and SiO_2 in Figure 2(a) and Figure 2(c) reveal the smooth surface of oxides with few crystallites formed. However, the surface of the oxide supports turned rough and bulky after impregnation with Ni, due to the NiO crystallites formation on the catalysts surface. From Figure 2(d), it can be seen that small particles covered the surfaces of SiO_2, resulting in rougher surface. This is due to higher Ni-loading that caused the agglomeration of NiO particles and the poor dispersion of Ni o and the supports.

The structural properties of Al_2O_3, Ni/Al_2O_3., SiO_2 and Ni/SiO_2 catalysts analyzed by N_2 physisorption are summarized in Table 1. Generally, Ni/Al_2O_3 possessed higher BET surface area compared to the Ni/SiO_2 since the surface area of the parent support of Al_2O_3 was higher than SiO_2. The BET surface area of the support SiO_2 and Al_2O_3 increased after introduction of Ni. This was probably caused by Ni, which contributes to a better dispersion of the particles. Similar results were also found by Diaz et al. [16] and Guo et al. [17]. The average pore diameter of Al_2O_3 and SiO_2 support slightly increased upon the addition of Ni. This could be as a result of the decomposition of $Ni(NO_3)_2.6H_2O$ after calcination leading to the formation of other porous structures. The pore volume increased upon addition of Ni due to the agglomeration of NiO species.

Table 1 BET surface area and pore volume of Al_2O_3, Ni/Al_2O_3, SiO_2 and Ni/SiO_2.

Catalyst	Surface area ($m^2\ g^{-1}$)	Pores volume ($cm^3\ g^{-1}$)	Pores diameter (Å)
Al_2O_3	0.85	0.00079	36.95
Ni/Al_2O_3	6.34	0.01600	31.89
SiO_2	0.40	0.00090	90.09
Ni/SiO_2	5.23	0.01130	29.24

TGA profiles of Ni/Al_2O_3 and Ni/SiO_2 presented in Figure 3 shows three stages of weight loss between 300 and 600 K. The initial weight loss region noticed at 300 K to 400 K was due to the removal of water vapour from the catalysts [18]. Consequently, weight loss was discovered between 400 and 500 K, indicative of the presence of two peaks which resulted from the removal of H_2O from $Ni(NO_3)_2.6H_2O$ as shown in Equation 5.

$$Ni(NO_3)_2.6H_2O \rightarrow Ni(NO_3)_2 + 6H_2O \quad (5)$$

The third stage weight loss from 500 K to 600 K indicates the decomposition of $Ni(NO_3)_2$ into NiO as in Equation 6. This results agrees with the findings reported by Estelle et al [19].

$$Ni(NO_3)_2 \rightarrow NiO + N_2O_5 \quad (6)$$

Temperature programmed reduction (TPR) was conducted to study the reducibility of the catalysts as well as to determine the suitable temperature for catalysts activation prior to reaction study. Figure 4 (a) shows the TPR profiles of Al_2O_3 and Ni (15)/Al_2O_3, respectively, while Figure 4 (b) shows the TPR profiles of SiO_2 and Ni (15)/SiO_2, respectively. From Figure 4, the reduction peaks of Ni (15)/Al_2O_3 can be found at 696 K. The peak indicates the reduction of NiO to Ni^o (refer to Equation 4.3) in which the interaction between NiO and Al_2O_3 is weak [20]. From Figure 4 (b), the reduction peak for Ni (15)/SiO_2 is at 652 K and relates to the

reduction of NiO to Ni° as well. This finding is consistent with the findings of Acrotumapathy et al. [21].

$$NiO + H_2 \rightarrow Ni + H_2O \quad (7)$$

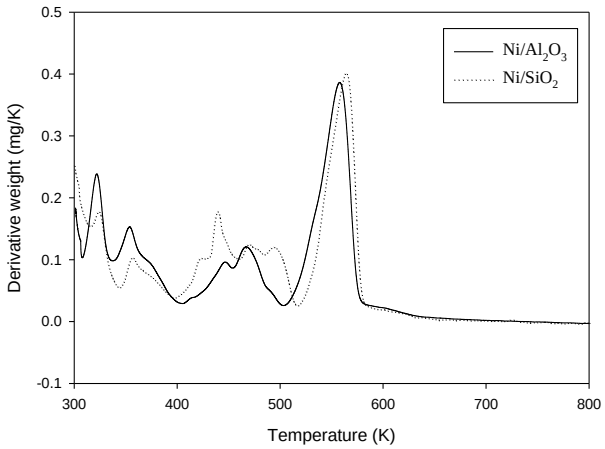

Figure 3 TGA analysis of catalysts at 10 K min^{-1} ramping rate in air blanket.

Ni (15)/SiO_2 has lower reduction temperature compared to Ni (15)/Al_2O_3 which shows that Ni (15)/SiO_2 is easier to be reduced compared to Ni (15)/Al_2O_3 due to the weaker metal-support interaction in Ni (15)/SiO_2 compared to Ni (15)/Al_2O_3. From the graphs, the designated temperature of catalyst reduction was chosen to be at 873 K, since all NiO species located on the catalyst surface were completely reduced to Ni° phase. In addition, the Al_2O_3 (cf. Figure 4 (a)) did not show any reduction peak which indicates that the reduction of pure oxide was difficult as a result of its stability [22]. Similar trend was observed for SiO_2 in Figure 4 (b).

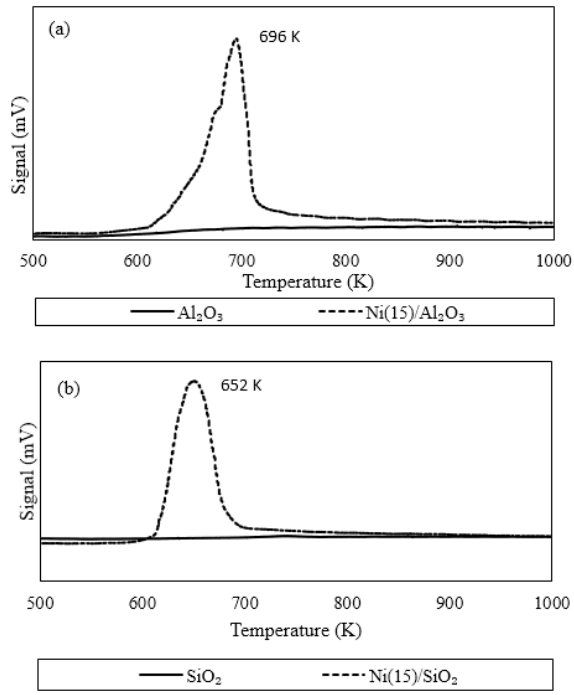

Figure 4 H_2-TPR profile of (a) Al_2O_3 and Ni/Al_2O_3, and (b) SiO_2 and Ni/SiO_2 catalysts at heating rate of 10 K min^{-1}.

TPR profiles of Ni/Al_2O_3 and Ni/SiO_2 is represented in Figure 4. The peak observed at 650 K and 700 K for both catalysts were due to the reduction of NiO to Ni°. This finding is consistent with the findings of Acrotumapathy et al. [21]. Ni/SiO_2 reduced at lower temperature and possessed lower H_2 uptake compared to Ni/Al_2O_3. However, both catalysts showed ability to easily reduce at relatively low temperature due to the strong O_2 storage capacity in the catalyst. From the analysis, it can be seen that the catalyst was completely reduced under H_2 flow at 750 K. Therefore, the reduction temperature of catalyst was set at 750 K during the reaction studies.

Temperature programmed desorption (TPD-NH_3) was conducted to characterize the surface acid strength of the catalysts post Ni impregnation. The acidity and basicity of a catalyst influences the interaction between reactants, the oxide and active metal sites. From the TPD-NH_3 analysis represented in Figure 5 (a) and Figure 5 (b), two distinct peaks were detected at different desorption temperature for both Ni (15)/Al_2O_3 and Ni (15)/SiO_2. The peak located at low desorption temperature range of 400 - 550 K belongs to the weak acid site, whilst the second peak observed at higher temperature above 625 K can be attributed to the strong acid center. For Ni (15)/Al_2O_3, the two peaks are located in weak acid region, while the peak for Ni (15)/SiO2 belongs to both weak and strong acid sites. The amount of NH_3 desorbed increased from 541.55 µmol g^{-1} to 4597.66 µmol g^{-1} with the addition of 15% Ni. It could be inferred that acid sites of the catalyst increased with the introduction of Ni. Hence, Ni (15)/Al_2O_3 is more acidic compared to Ni (15)/SiO_2. Interestingly, despite it's the amphoteric characteristic, silica has a weak strength of acidity [17]. The total amount of NH_3 absorbed for Ni (15)/SiO_2 was 403.10µmol g^{-1}. However, addition of Ni still increased the acidity on the surface of the catalyst, probably due to the ability of Ni to attract water and produce more acidic sites on the catalyst surface.

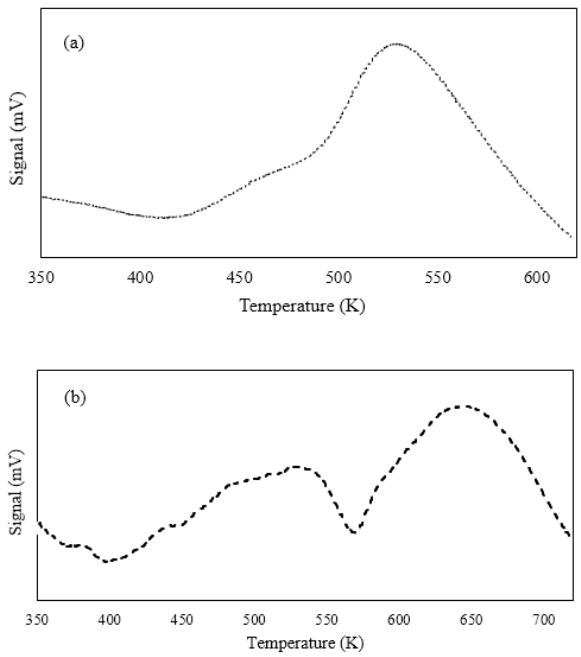

Figure 5 Temperature programmed desorption (TPD-NH_3) profiles of (a) Ni/Al_2O_3 and (b) Ni (15)/SiO_2

3.2 Reaction Study

The glycerol dry reforming was conducted in a fixed bed reactor at 973 K, for 3 h, in a 1:1 CO_2 to glycerol ratio under atmospheric pressure. Prior to the glycerol dry reforming, the blank run was carried out in the empty reactor at 973 K, CO_2: $C_3H_8O_3$ (CGR) of 1:1 under atmospheric pressure for 3 h. N_2 as carrier gas was fed into the reactor to achieve total flow rate of 120 ml min^{-1}. The GC analysis was used to detect H_2 and CO in the product stream, indicative of the decomposition of glycerol at the selected operating reaction conditions. Although, it is inevitable to eliminate the side reactions when operating at high reaction temperature, the glycerol conversion and H_2 yield obtained from the blank run test gave lower values (2.3% and 0.9%, respectively) compared to the glycerol conversion and H_2 yield obtained using catalysts. Hence, any improvement on the glycerol conversion and H2 yield during glycerol dry reforming with the presence of the Ni-based catalyst was due to the physicochemical properties and efficiency of the catalyst.

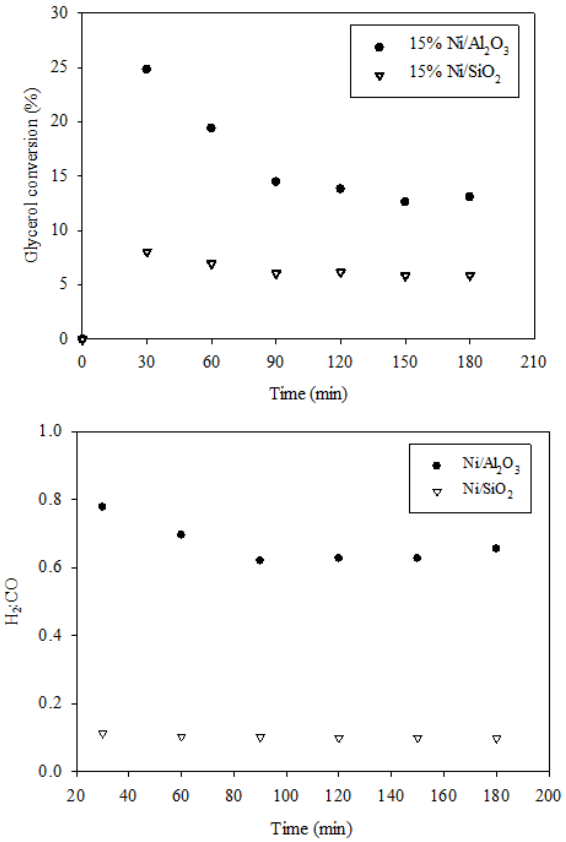

Figure 6 (a) Glycerol conversion and (b) H_2: CO products ratio over catalysts for 3 hours reaction time [Reaction conditions: T=973 K, P=1 atm and CO_2: Glycerol of 1:1]

Figure 6(a) shows the glycerol conversion over Ni/Al_2O_3 and Ni/SiO_2 for 3 h time on stream. For both catalysts, the glycerol conversions increased for the first 0.5 h and stable after 1.5 h of reaction. This can be ascribed to the deposition of carbonaceous species on the catalyst surface upon breakage of C - C bond in glycerol. The glycerol conversion over Ni/Al_2O_3 is much higher than Ni/SiO_2 with the value of 14.46% and 6.94%, respectively. This result is attributable to the higher surface area of Ni/Al_2O_3 which provides a better interaction between Ni active sites and glycerol during the reaction. Furthermore, the presence of small particles in Ni/SiO_2 as disclosed in the XRD analysis resulted in catalyst blockage and lowered the reactant conversion. H_2: CO ratio over both catalysts were presented in Figure 6 (b). A low H_2: CO ratio is preferable for some processes such as the production of aldehydes [7].

The gaseous products yield i.e. H_2, CH_4 and CO obtained over Ni/Al_2O_3 and Ni/SiO_2 catalysts are shown in Figure 7. The H_2 yield of Ni/Al_2O_3 (9.82%) is higher compared to Ni/SiO_2 (3.27%). It can be deduced that from the figure, CH_4 yield is apparently lower than the yield of H_2 and CO in the consecutive run. These results might be due to the contribution of CH_4 in deposition of carbonaceous species during the reaction. Similar observation was reported by Jeong and Kang (2010) where CH_4 was formed via dehydrogenation of glycerol which at the same time contributes to the deposition of carbonaceous species [23]. CO yield is in excess for both the catalysts, approximately 4 times the yield of H_2.

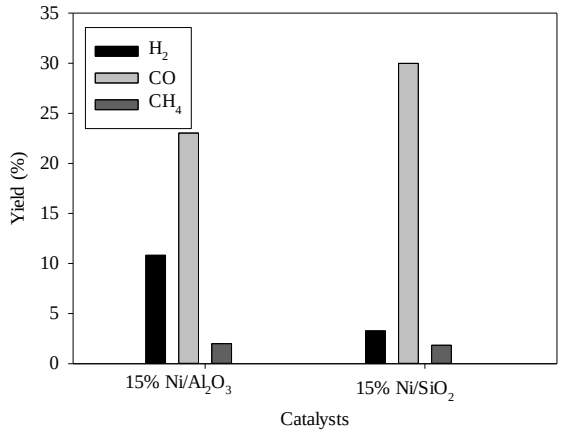

Figure 7 Hydrogen, methane and carbon monoxide yield [Reaction conditions: T=973 K, P=1 atm and CO_2: Glycerol of 1:1]

3.3 Characterization of Used Catalyst

TPO analysis was conducted to evaluate the amount of coke deposition on the surface of used catalysts for the post-reaction of glycerol dry reforming. The profile represented in Figure 8, shows increased in catalysts' weight during the TPO analysis symptomatic of the formation of carbon oxidized on the catalyst surfaces. Similar observation was reported by Wu and Williams [24] and Wu et al. [25]. The oxidation peak for Ni/Al_2O_3 at 793 K can be linked to the formation of encapsulated carbon on the catalysts surface [25]. Although, catalytic reaction study of Ni/Al_2O_3 resulted in higher glycerol conversion and H_2 yield. Interestingly, Ni/SiO_2 had lower coke deposition likely due to the type of carbon deposited on the catalyst's surface (filamentous carbon). The formation of filamentous type of carbon at 848 K for Ni/SiO_2 can be related to the formation of carbon nanotubes, which usually occur at 883 K [24].

The SEM result reveals the presence of carbon deposit on the catalysts. Two types of carbon deposit; encapsulating carbon and filamentous carbon, represented in Figure 9 were captured. In addition, Figure 9 (a) representing the spent Ni/Al_2O_3 showed that the solid carbon formed small particles, which encapsulated the active sites of the catalysts. Figure 9 (b) shows the whisker-like or filamentous type of carbon deposit found in Ni/SiO_2. As revealed in the TPO analysis, the

encapsulated carbon in Ni/Al_2O_3 was formed at higher temperature compared to filamentous carbon in Ni/SiO_2. Compared to filamentious carbon, encapsulated carbon have the higher risk to affect the catalyst stability as it might cover the active sites of the catalyst [26]. The large catalyst particles of SiO_2 contributes to the formation of encapsulated carbon while small catalyst particles contribute to the formation of filamentous carbon on the spent catalyst surface [27]. As reported by De Oliveira-Vigier et al., filamentous carbon possess metal particles on its tip during reaction [28]. The carbon deposit on the catalyst surface could also contribute to the explanation of the superior catalytic activity of Ni/Al_2O_3 compared to Ni/SiO_2.

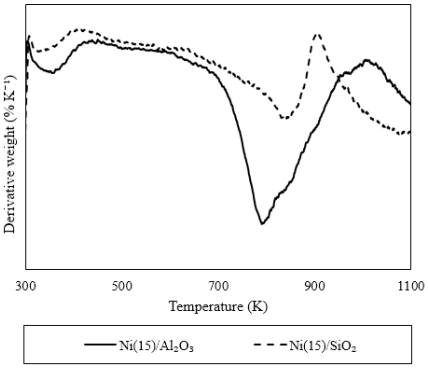

Figure 8 TPO results of spent catalysts at 10 K min^{-1} ramping rate in air blanket.

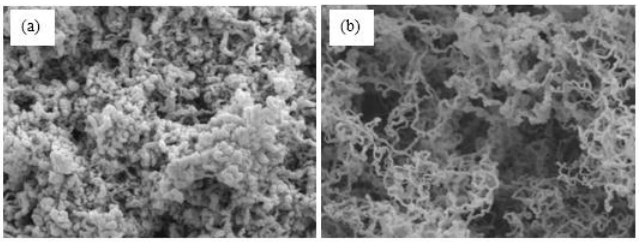

Figure 9 SEM image of the spent catalyst at 30,000x magnification. (a) encapsulated carbon deposition (b) filamentous carbon

4.0 CONCLUSION

From the experimental analysis, glycerol dry reforming successfully produced syngas (H_2: CO) with H_2: CO ratio less than 1 which is suitable to be utilized in the production of chemicals such as aldehydes. The glycerol conversions over Ni/Al_2O_3 and Ni/SiO_2 were 14.46% and 6.94%, respectively. Ni/Al_2O_3 gave the optimum glycerol conversion and H_2 yield of 14.46% and 11.45%, respectively. The performance can be linked to higher BET surface area of Ni/Al_2O_3 as compared to Ni/SiO_2. XRD analysis revealed that small NiO particles were formed on Ni/Al_2O_3. SEM analysis showed evidence of the formation of NiO particles on the surface of fresh catalyst that indicates the presence of active sites of the catalyst. The morphology captured via SEM images showed the formation of small particles on the catalyst support, well dispersed on the Ni (15)/Al_2O_3. In addition, Ni (15)/SiO_2 showed the encapsulation of Ni particles on the support which minimised the catalyst surface area. Both catalysts possessed similar behaviour in the TPC analysis, which indicates that the metal precursors in both catalysts can be decomposed at temperature around 773 K. From TPR analysis, Ni (15)/Al_2O_3 has stronger Ni and support interaction than Ni (15)/SiO_2, thereby leading to better reducibility of Ni(15)/SiO_2 at lower temperature. Although Ni(15)/SiO_2 has lower acidity compared to Ni (15)/Al_2O_3, the reactivity was also relatively lower. The deposition of encapsulated carbon on the catalyst surface was not severe, as the glycerol conversion and product yield remain consistent throughout the reaction time.

ACKNOWLEDGEMENTS

Authors would like to thank Ministry of Education Malaysia for awarding the FRGS research grant vote RDU130108 and Universiti Malaysia Pahang for financial support.

REFERENCES

[1] N. Kolesarova, M. Hutnan, I. Bodik, V. Spalkova, J. Biomed. Biotechnol 201 (2011) 1110.
[2] C.K. Cheng, R.H. Lim, A. Ubil, S.Y. Chin, J. Gimbun, Adv. Mater. Phys. Chem 2 (2012) 165.
[3] Y. Lin, Int. J. Hydro. Energy 38 (2013) 2678.
[4] K. Goransson, U. Soderlind, J. He,W. Zhang, Ren. Sust. Energ. Rev 15 (2011) 482.
[5] X. Wang, M. Li, M. Wang, H. Wang, S. Li, S. Wang, X. Ma, Fuel 88(2009) 2148.
[6] Y. Li, W. Wang, B. Chen, Y. Cao, Int. J. Hydro. Energy 35 (2010) 7768.
[7] K.W. Siew, H.C. Lee, J. Gimbun, C.K. Cheng, Int. J. Hydro. Energy 39 (2014) 6927.
[8] K.W. Siew, H.C. Lee, J. Gimbun, C.K. Cheng, Bulletin of Chemical Reaction Engineering & Catalysis 8 (2013) 160.
[9] K.W. Siew, H.C. Lee, J. Gimbun, C.K. Cheng, J. Energ. Chem 23 (2014) 15.
[10] H.C. Lee, K.W. Siew, J. Gimbun, C.K. Cheng, Bulletin of Chemical Reaction Engineering & Catalysis 8 (2013) 137.
[11] H.C. Lee, K.W. Siew, J. Gimbun, C.K. Cheng, Chem Eng J 255 (2014) 245.
[12] T. Shirai, H. Watanabe, M. Fuji, M. Takahashi, Ceramic Foundation Engineering Research Center Annual Report, 9 (2009) 23.
[13] J.R.H. Ross, V.N.J. van Keulen, M.E.S. Hegarty, K. Seshan, Catal. Today 30 (1996) 193.
[14] A.L. Patterson. Physic. Review 56 (1939) 978.
[15] A. Ebshish, Z. Yaakob, B. Narayanan, A. Bshish, W.R. Wan Daud, Int J of Integrated Eng. 3 (2011) 5.
[16] G.C. Diaz, N.C.O. Tapanes, L.D.T. Camara, D.A.G. Aranda, Renew Energy 64 (2014) 113.
[17] J. Guo, Hou Z, Gao J, Zheng X, Fuel 87 (2008) 1348.
[18] F.H. Alhassan, U. Rashid, M.S. Al-Qubaisi, A. Rasedee, Y.H. Taufiq-Yap, Powder Technol 253 (2014) 809.
[19] J. Estellé, P. Salagre, Y. Cesteros, M. Serra, F. Medina,J.E. Sueiras, Solid State Ionics 156 (2003) 233.
[20] I.N. Buffoni, F. Pompeo, G.F. Santori, N.N. Nichio, Catal. Comm., 13 (2009) 1656.
[21] V. Acrotumapathy, N.V. Dai-Viet, D. Chesterfield, T.T. Cao, A. Siahvashi, F.P. Lucien, A.A. Adesina, Appl Catal A-Gen 479 (2014) 87.
[22] C.A. Pires, A.C.C. dos Santos, E. Jordao, Braz J Chem Eng, 32 (2014) 837.
[23] H. Jeong, M. Kang, Appl Catal B-Environ 95 (2010) 446.
[24] C. Wu, Z. Wang, P.T. Williams, J. Huang, Scientific Report 3 (2013) 2742.
[25] C. Wu, P.T. Williams, Appl Catal B-Environ 87 (2009) 152.
[26] V. Chiodo, S. Freni, A. Galvagno, N. Mondello, F. Frusteri, Appl. Catal. A-Gen 381 (2010) 1.
[27] G. Bonura, O. Di Blasi, L. Spadaro, F. Arena, F. Frusteri. Catal. Today 1 (2006) 77.
[28] K. De Oliveira-Vigier, N. Abatzoglou, F. Gitzhofer. Can. J. Chem. Eng., 83 (2005), 978.